Rapid Communications

Empirical way for finding new uranium-based heavy-fermion materials

E. Svanidze, A. Amon, R. Borth, Y. Prots, M. Schmidt, M. Nicklas, A. Leithe-Jasper, and Yu. Grin
Max-Planck-Institut für Chemische Physik fester Stoffe, Nöthnitzer Straße 40, Dresden 01187, Germany

(Received 1 August 2018; revised manuscript received 17 May 2019; published 17 June 2019)

The field of heavy-fermion physics emerged nearly four decades ago and has since remained one of the most prominent research directions in condensed-matter physics. Nonetheless, while significant progress has been made in unraveling heavy-fermion behavior and accompanying exotic phenomena, many questions remain. This issue can be advanced from two directions: comprehensive understanding of existing materials and discovery of novel systems. In this work, we propose a targeted method for discovery of uranium-based heavy-fermion materials by synthesis of complex intermetallic compounds with low mass percentage of uranium, high coordination number of uranium, and long overall shortest uranium bond length. We report the discovery and synthesis of the new complex uranium-based heavy-fermion material $U_{23}Hg_{88}$, which suggests this approach to be a reliable route for the targeted search of novel strongly correlated uranium-based materials. The Sommerfeld coefficient $\gamma = 630$ mJ mol$_U^{-1}$ K^{-2} indicates extremely strong electronic correlations and places $U_{23}Hg_{88}$ among the heaviest uranium-based compounds. $U_{23}Hg_{88}$ orders antiferromagnetically below $T_N = 2.2$ K and displays a dual nature of the 5*f* electrons. This work will pave a way for a comprehensive understanding of heavy-fermion phenomena in general and uranium-based systems in particular.

DOI: 10.1103/PhysRevB.99.220403

Actinide- and lanthanide-based strongly correlated materials exhibit a wide range of peculiar properties: unconventional superconductivity and quantum criticality, coexistence of superconductivity and magnetism, complex magnetic configurations, hidden order, as well as heavy-fermion and non-Fermi-liquid behaviors [1–15]. Not surprisingly, these intriguing materials can be easily perturbed by chemical substitution, magnetic field, or pressure, frequently revealing puzzling phase diagrams. Deviations from theoretical predictions are often observed in the vicinity of the emergent ground states and thought to arise from partial localization of *f* electrons, driven by an interplay between the hybridization of the 4*f* or 5*f* states with the conduction electrons and the local Coulomb correlations [16].

Compared with cerium- and ytterbium-based materials, fewer uranium-based heavy-fermion systems are known [1–3,13]. Moreover, the vast majority of uranium-based compounds display comparatively small values of the Sommerfeld coefficient γ, as can be seen from Fig. 1. The fundamental reason behind such a considerable difference in electron mass enhancement of 4*f* vs 5*f* compounds is not yet clear, which can perhaps be attributed to the complexity and scarcity of uranium-based heavy-fermion systems. Given the intricacy of uranium-based materials from a computational point of view, more experimental investigations will likely shed light on this matter.

In search of new uranium-based heavy-fermion compounds, we have examined the existing systems: among unperturbed compounds, the highest values of γ are observed in UPt_3 ($\gamma = 420$ mJ mol$_U^{-1}$ K^{-2} [1]), U_2Zn_{17} ($\gamma = 450$ mJ mol$_U^{-1}$ K^{-2} [17]), UPd_2Al_{20} ($\gamma = 500$ mJ mol$_U^{-1}$ K^{-2} [18]), and UCd_{11} ($\gamma = 840$ mJ mol$_U^{-1}$ K^{-2} [19,20]). From Fig. 1(a) it is evident that atomic concentration does not affect the Sommerfeld coefficient γ: moderately heavy ($\gamma < 200$ mJ mol$_U^{-1}$ K^{-2}), intermediately heavy ($200 \leqslant \gamma < 400$ mJ mol$_U^{-1}$ K^{-2}), and exceptionally heavy ($\gamma \geqslant 400$ mJ mol$_U^{-1}$ K^{-2}) compounds cover a large span of U coordination and atomic concentration. The effect of atomic [Fig. 1(a)] and mass [Fig. 1(b)] concentrations of U is drastically different: not only should uranium atoms be diluted, but it is more beneficial to mix heavier elements with uranium, if we want to observe heavy-fermion behavior. This gives us a first clue as to where we can find uranium-based heavy-fermion systems – compounds with uranium coordination number above 12 and mass percentage under 40% should be considered. We then proceed to examine features of chemical bonding in uranium-based materials, as this has been shown to have a strong influence on their ground-state properties [30]. It is clear from Fig. 1(c) that the shortest uranium-uranium bond does not affect the Sommerfeld coefficient, while some enhancement is driven by an increase of coordination. We now examine the overall shortest uranium bond, i.e., the shortest distance between a uranium and a nonuranium atom. From Fig. 1(d), we notice that for the majority of uranium-based compounds with an exceptionally heavy electron mass, this distance is above 3 Å.

By examining several characteristics of known uranium-based heavy-fermion materials we can postulate three key ingredients that will likely lead to the discovery of new uranium-based heavy-fermion systems: (i) mass percentage of uranium should be below 40%, (ii) coordination number of uranium should be above 12, and (iii) the overall shortest uranium bond should be above 3 Å.

There are even more similarities between two heaviest uranium-based materials UCd_{11} and U_2Zn_{17}. Both systems order antiferromagnetically, with uranium-uranium distances

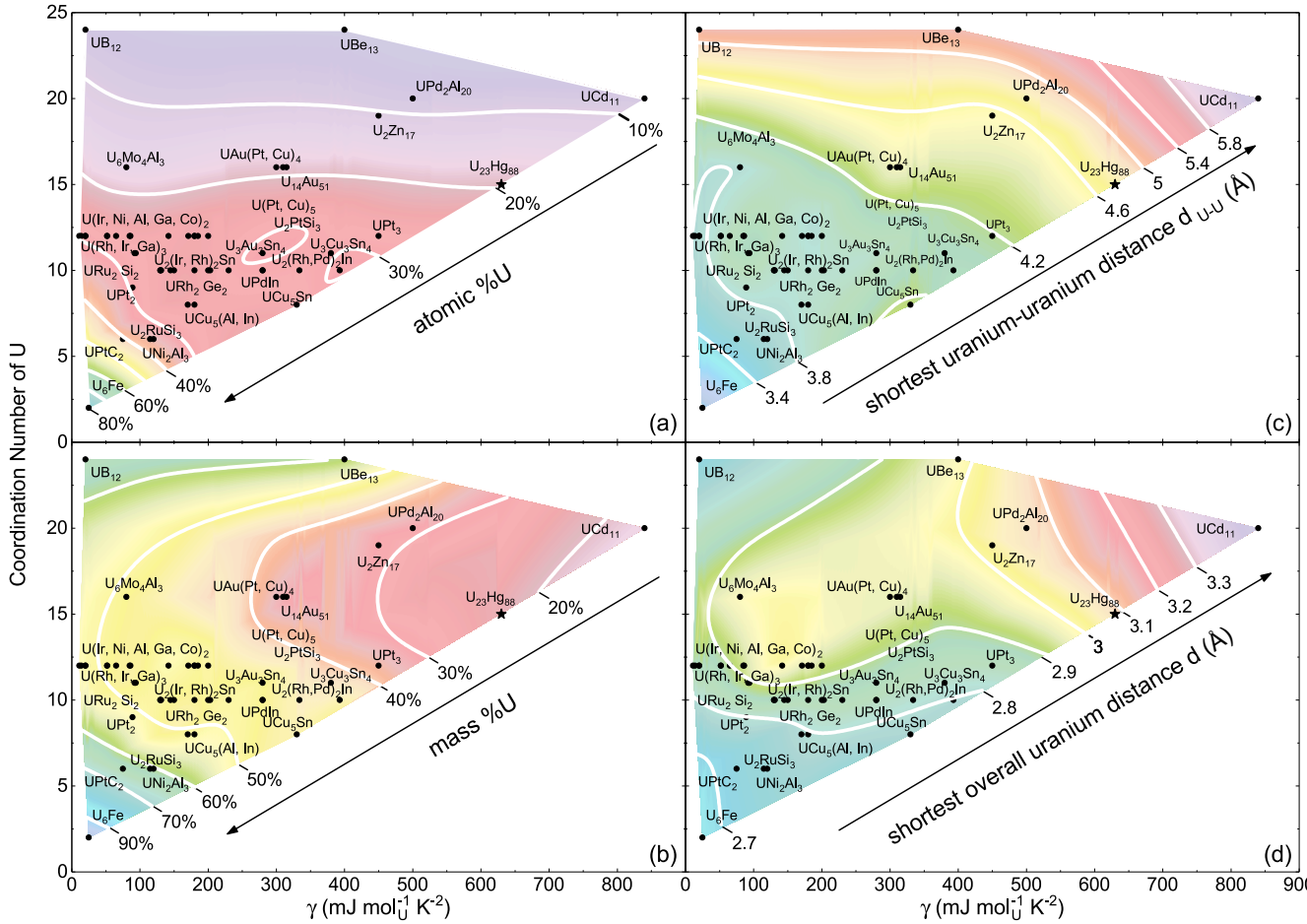

FIG. 1. Coordination number of uranium as a function of Sommerfeld coefficient γ for uranium-based heavy-fermion compounds. The color represents (a) atomic percent uranium, (b) mass percent uranium, (c) length of the shortest uranium-uranium bond, and (d) length of the overall shortest uranium bond for each of the compounds. The newly discovered compound $U_{23}Hg_{88}$ is marked by a star symbol.

above the Hill limit [30], highly coordinated uranium atoms with complex unit cells, and are composed of uranium and column IIB atoms Zn or Cd. In hopes of reproducing the strong hybridization of uranium *f* electrons, which is likely responsible for such a considerable effective mass enhancement, we have assessed the U-Hg phase diagram. The initial interest in the U-Hg system was driven by the intention of recovering U from spent nuclear fuels via amalgamation [31–33]. This was also thought to be an avenue toward enhancing the purity of U metal itself [34–39]. However, it was quickly realized that all U-Hg compounds are extremely air sensitive [40–43], which limits their industrial applications. This can possibly explain the small number of studies pertaining to the physical properties of the U-Hg phases. Nonetheless, several U-Hg compounds were discovered and characterized from the crystallographic point of view: hexagonal UHg_2 [33,40–48] and UHg_3 [33,40–44,46–48], as well as cubic $U_{11}Hg_{45}$ [49], which was previously thought to be UHg_4 [33,40–42,46,47,50,51]. UHg was suggested to crystallize in a hexagonal lattice [46,48]. Due to conflicting reports regarding physical properties of the U-Hg phases [45,51–53], we have synthesized polycrystalline samples of $U_{23}Hg_{88}$, UHg_3, and UHg_2 and several other stoichiometries [see Supplemental Material Fig. S1(a)] [54]. The preparation of these materials in high-purity single-phase form was exceptionally challenging, due to the extreme air and moisture sensitivity of all U-Hg phases. The solution of these issues, along with further experimental details, are summarized in the Supplemental Material [54].

In this work, we present the discovery and characterization of a novel antiferromagnetic heavy-fermion compound $U_{23}Hg_{88}$. This system exhibits an exceptionally large electronic specific heat coefficient $\gamma = 630$ mJ mol$_U^{-1}$ K^{-2}. $U_{23}Hg_{88}$ fulfills all three criteria listed above: (i) the uranium mass percentage is 21%, (ii) the average uranium coordination is 15, and (iii) the overall shortest uranium bond is a uranium-mercury one with length of 3.12 Å. $U_{23}Hg_{88}$ is the first successful example of a novel system found using these empirical parameters, suggesting a route for forthcoming discoveries.

The crystal structure of the investigated compound was previously assigned to the $Sm_{11}Cd_{45}$ structure type (space group $F\bar{4}3m$, 448 atoms in the unit cell) [49]. Despite the fact that the x-ray powder diffraction pattern was indexed completely using the cubic F-centered unit cell with $a = 21.7172(7)$ Å, our attempt to calculate the intensities of reflections reveals marked deviations from the experiment.

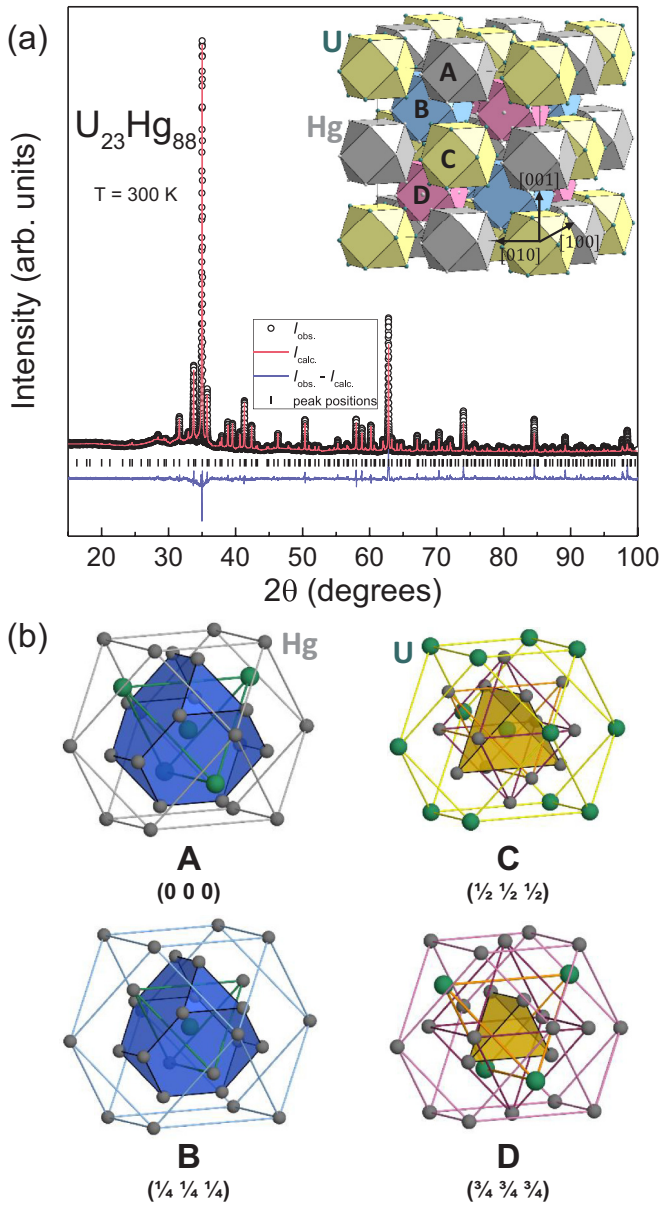

FIG. 2. Crystal structure of $U_{23}Hg_{88}$: (a) X-ray powder diffraction pattern (Cu$K\alpha_1$ radiation, $\lambda = 1.54056$ Å) with I_{obs}, I_{calc}, and $I_{obs} - I_{calc}$ represented by black circles and red and blue lines, respectively. The black ticks mark peak positions for the space group $F\bar{4}3m$. Inset: arrangement of the four types of nested polyhedra units in the unit cell [A (gray), B (blue), C (yellow), and D (pink)]. (b) Constitution of the 29- (A and B), 27- (C), and 26-atom (D) polyhedra units. U and Hg atoms are represented by green and gray spheres, respectively.

Upon further refinement, the occupation of the position at (3/4, 3/4, 3/4) was reduced toward zero, and the calculated difference Fourier maps suggest at least one additional position missing in comparison with the $Sm_{11}Cd_{45}$ model. The newly obtained model also yields good agreement between the calculated and experimental intensities of the x-ray powder diffraction data see Fig. 2(a)]. Both experiments are strongly hindered by the high chemical reactivity of the material and high linear absorption coefficient of the components. In particular, distinguishing between U and Hg in the crystal structure was difficult due to their similar scattering factors and atomic radii. Crystallographic data are listed in Supplemental Material Tables S1–S3, with the further study of structural details currently underway.

Similarly to the previously described Pt_5Be_{21} [55] and $Sm_{11}Cd_{45}$ [56], the crystal structure of $U_{23}Hg_{88}$ can be crystallographically derived from a $6 \times 6 \times 6$ superstructure of the bcc pattern with a distinct distribution of defects and local distortions, caused by the latter. Four nested polyhedron units are necessary to describe the crystal structure. Unit A is centered at the U2 atom at (000) and contains 28 atoms—U@$Hg_{24}U_4$. Unit B (U@Hg_{28}) is built around U3 at (1/4, 1/4, 1/4). Unit C is formed around U1 atoms at (1/2, 1/2, 1/2) and has composition U@$Hg_{14}U_{12}$. The center of the unit D blank (□@$Hg_{22}U_4$) at (3/4, 3/4, 3/4) is not occupied. In the unit cell, A, B, C, and D are arranged according to the bcc pattern [inset of Fig. 2(a)]. Due to the total composition being close to UHg_4, the local coordination of U atoms is governed by Hg; the coordination numbers of uranium are 14 and 16. Both U_2Zn_{17} and UCd_{11} also show high coordination numbers of the U atoms—13 [57] and 20 [58], respectively, which is perhaps related to essential effective mass enhancement observed in these systems. Moreover, structural complexity can be quantified using the number of atoms per primitive unit cell N, with values over $N = 100$ marking complex crystal structures [59,60]. With 111 atoms in the primitive cell $U_{23}Hg_{88}$ belongs to the same structure family. This value is significantly higher than that of UPt_3 ($N = 8$), U_2Zn_{17} ($N = 17$), UPd_2Al_{20} ($N = 46$), and even UCd_{11} ($N = 36$). The coordination number reflects chemical interactions in an indirect way. While other parameters must be considered in the bonding description, we provide an initial assessment of several features of all known uranium-based materials. A comprehensive analysis of all bonding descriptors and their correlation with the heavy-fermion behavior by means of an in-depth theoretical investigation is highly desired.

One of the central questions for heavy-fermion materials is the state of the 5f electrons. The modified Curie-Weiss fit of the magnetic susceptibility data for $U_{23}Hg_{88}$, with the temperature-independent contribution $M_0/H = 1.1 \times 10^{-5}$ emu mol_U^{-1} subtracted, is shown in Fig. 3(a). The resultant effective moment $\mu_{\text{eff}} = 3.43\mu_B$ U^{-1} signals localized nature and weak hybridization of the 5f electrons at high temperature. The antiferromagnetic transition is evidenced by a characteristic cusp, with identical zero-field-cooled and field-cooled curves [Fig. 3(b)]. The value of the Néel temperature $T_N = (2.2 \pm 0.1)$ K is estimated from the derivative of magnetization $d(MT)/dT$ and specific heat C_p/T data, similar to what has been done for other antiferromagnetic materials [61]. The large and negative value of the Weiss temperature $\theta_W = -90$ K supports an antiferromagnetic Kondo scenario [62] with $T_K = N_A\mu_{\text{eff}}^2/[3k_BM/H(0)] = (90 \pm 10)$ K. However, this method likely overestimates the value of the Kondo temperature T_K due to the lack of saturation in the magnetic susceptibility of $U_{23}Hg_{88}$ [Fig. 3(b)]. It is therefore possible that $T_K \approx 50$ K, as the inverse susceptibility data deviate from linearity around this temperature [Fig. 3(a)].

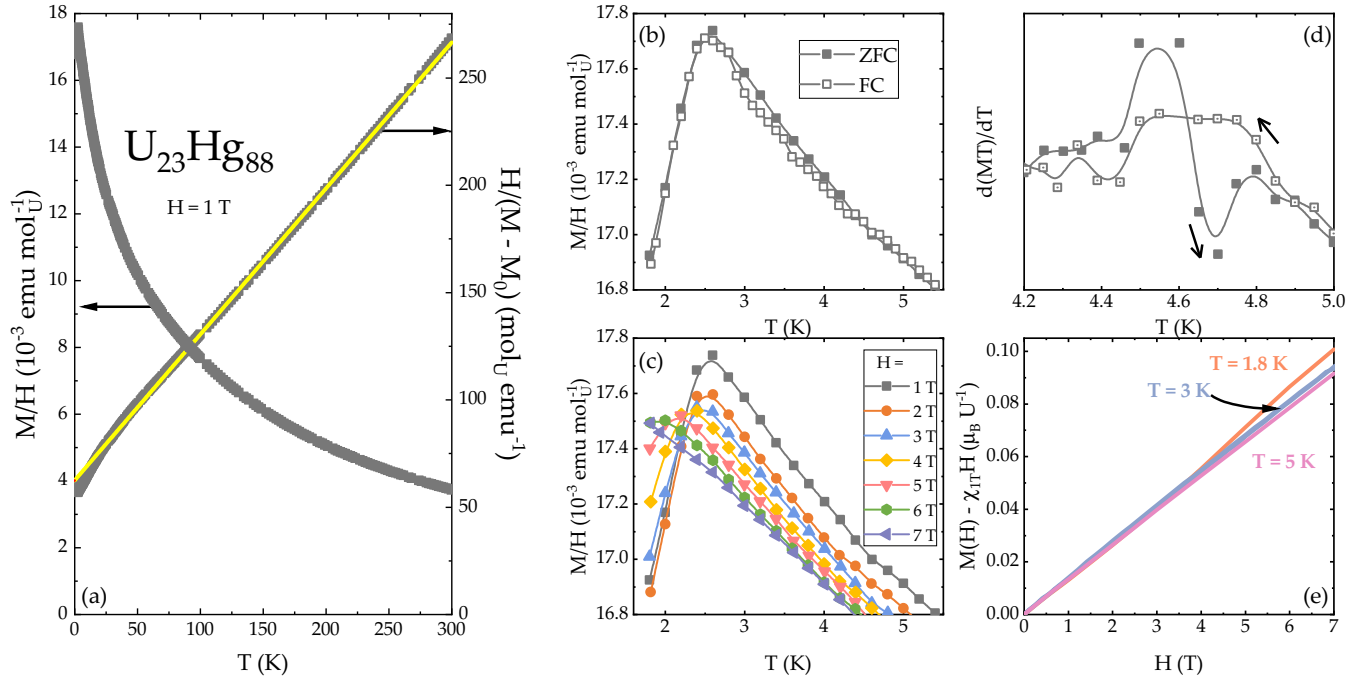

FIG. 3. Magnetic properties of $U_{23}Hg_{88}$: (a) Magnetic susceptibility M/H (left axis) along with the inverse magnetic susceptibility $H/(M - M_0)$ (right axis) as a function of temperature for $H = 1$ T. The modified Curie-Weiss fit is represented by a solid line. (b) The zero-field-cooled (full symbols) and field-cooled (open symbols) M/H. (c) Evolution of the antiferromagnetic transition as a function of the applied field for $0 \leqslant H \leqslant 7$ T. (d) Temperature derivative of magnetic susceptibility $d(MT)/dT$ taken on warming (full symbols) and on cooling (dotted symbols) in $H = 1$ T. (e) The magnetic isotherms, with the linear component subtracted $M(H) - \chi_{1T}H$, for $T = 1.8$ K (orange), $T = 3$ K (blue), and $T = 5$ K (pink).

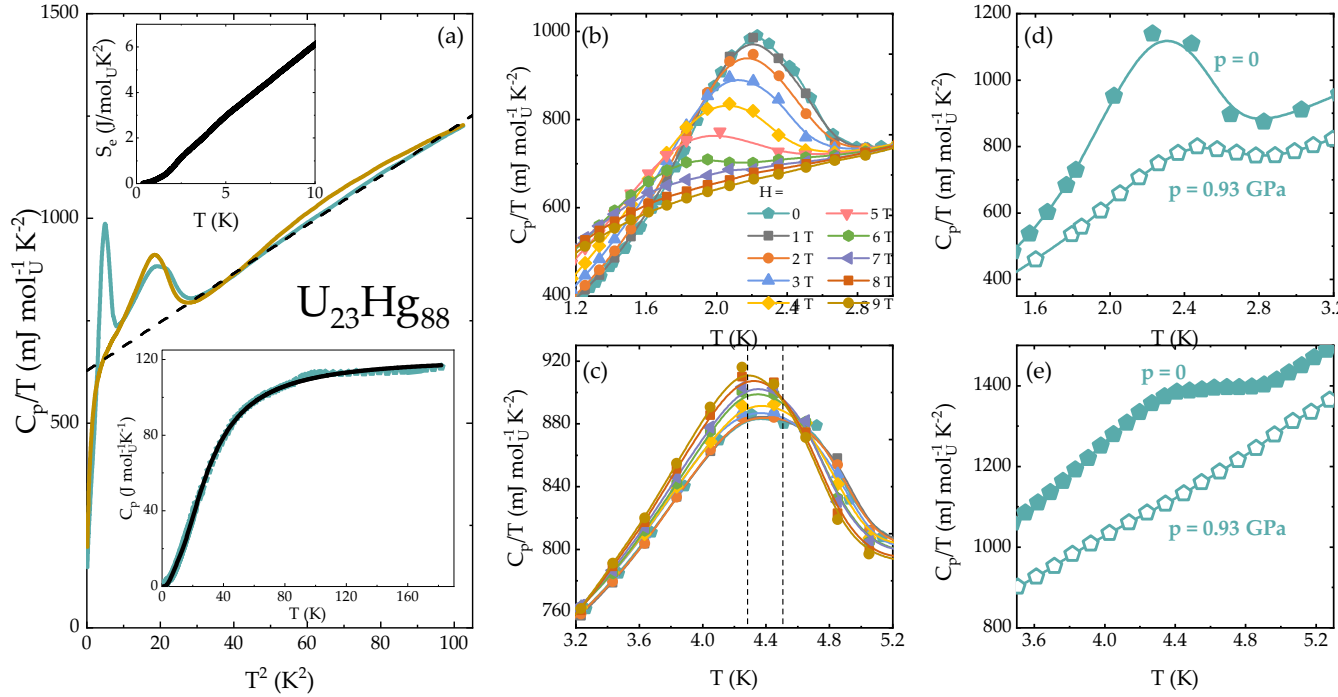

FIG. 4. Specific heat data for $U_{23}Hg_{88}$: (a) Specific heat C_p/T as a function of T^2 for $U_{23}Hg_{88}$ in $H = 0$ (green line) and $H = 9$ T (brown line) along with a linear fit (dashed line). The fit is used to estimate $\gamma = 630$ mJ mol$_U^{-1}$ K^{-2} and the entropy of conduction and magnetic $5f$ electrons, which is dominated by the $5f$ contribution, S_e (top inset) (since a nonmagnetic analog $Th_{23}Hg_{88}$ does not exist). Bottom inset: Specific heat in the high-temperature region, along with phonon contribution, calculated using the Debye-Einstein fit (solid line). Application of magnetic field suppresses the antiferromagnetic transition, as shown in (b), while the T_s transition remains field independent up to $H = 9$ T, as evident from (c). Specific heat data taken in zero pressure (solid symbols) and in $p = 0.93$ GPa (open symbols). The antiferromagnetic transition is weakly affected by the application of pressure [panel (d)], while the T_s transition is easily suppressed by it [panel (e)].

At low temperatures, $U_{23}Hg_{88}$ evolves continuously into a heavy Fermi-liquid ground state with $C_p/T \propto T^2$ [Fig. 4(a)]. This yields $\gamma = 630$ mJ mol$_U^{-1}$ K^{-2}, which is not affected by application of a magnetic field. However, a small field-induced broadening is evident, the origin of which is not yet known. At high temperatures, the specific heat data can be fit with a Debye-Einstein fit [$\Theta_D = (30 \pm 3)$ K, $\Theta_E = (100 \pm 5)$ K] [18], as shown in the bottom inset of Fig. 4(a). At the antiferromagnetic transition, the 5*f* entropy is rather small. This, together with a high value of the Sommerfeld coefficient $\gamma = 630$ mJ mol$_U^{-1}$ K^{-2} [Fig. 4(a)], the reduction of γ below T_N, and the absence of a feature associated with the transition in the resistivity data [Fig. 5(a)], favor an itinerant magnetic moment scenario. The coexistence of local and itinerant magnetic moment signatures suggests a dual nature of 5*f* electrons in $U_{23}Hg_{88}$.

In addition to the $T_N = 2.2$ K antiferromagnetic ordering of $U_{23}Hg_{88}$, another transition takes place at $T_s = 4.4$ K, as evident from the specific heat data [Figs. 4(a) and 4(c)]. There is a weak thermal hysteresis associated with the T_s transition, observed in magnetic susceptibility [Fig. 3(d)], which indicates that this transition is likely first order. Most certainly, the T_s transition does not have a magnetic component, since the magnetic isotherms, taken at $T = 3$ K and $T = 5$ K [Fig. 3(e)], are quite similar, even after the linear component has been subtracted. Furthermore, the application of a magnetic field affects the transition temperature T_s very slightly, as visible from Fig. 4(c). Overall, the value of T_s changes only by $\Delta T_s = 0.1$ K over the whole field range [Fig. 5(b)]. Therefore, this transition is likely of a structural character, given the thermal hysteresis [Fig. 3(d)] and small entropy of this transition [Fig. 4(a)]. Additionally, the value of the Debye temperature Θ_D, extracted from the high-temperature specific heat fit [Fig. 4(a)], amounts to only $\approx$30 K. This value is in good agreement with that obtained from the slope of the C_p/T vs T^2 data at low temperature: $\Theta_D = 47$ K. Such low value of the Debye temperature is comparable to that of pure Hg ($\Theta_D = 72$ K [64]), attesting to the softness of the $U_{23}Hg_{88}$ system and supporting the possibility of a structural transition at T_s. Not surprisingly, the application of pressure $p = 0.93$ GPa [Fig. 4(e)], destroys this transition.

Contrary to the T_s transition, the antiferromagnetic transition of $U_{23}Hg_{88}$ is rather strongly affected by the application of a magnetic field, as shown in Fig. 3(c). The critical field, necessary to completely suppress the antiferromagnetic order, is estimated to be $H_c = 11.6$ T, as evident from the *H*-*T* phase diagram, shown in Fig. 5(b). The value of H_c is rather modest, especially considering critical fields of 20 T [65] and 33 T [66] for UCd_{11} and U_2Zn_{17}, respectively. On the other hand, the antiferromagnetic state of $U_{23}Hg_{88}$ is robust against the applied pressure of up to $p = 0.93$ GPa, as summarized in Fig. 4(d). While the entropy involved in the transition is reduced, the Néel temperature T_N increases from $T_N = 2.2$ K ($p = 0$) to $T_N = 2.4$ K ($p = 0.93$ GPa). The increase of the antiferromagnetic ordering temperature with pressure has also been observed for UCd_{11} [67] and U_2Zn_{17} [66]. The reason behind such an enhancement is not yet known, calling for additional investigations [68,69].

Surprisingly, among heavy-fermion systems with exceptionally high γ values, the distance between neighboring U atoms correlates with the value of γ. The value of $d_{U\text{-}U}$ for $U_{23}Hg_{88}$ ($d_{U\text{-}U} = 4.67$ Å) is in between that of U_2Zn_{17} and UCd_{11} [see Fig. 1(c)], and is also above the Hill limit ($d_{U\text{-}U} = 3.5$ Å [30]). This is consistent with $\gamma(U_2Zn_{17}) = 535$ mJ mol$_U^{-1}$ K^{-2} [17] $< \gamma(U_{23}Hg_{88}) = 630$ mJ mol$_U^{-1}$ K^{-2} [see Fig. 4(a) of the present work] $< \gamma(UCd_{11}) = 840$ mJ mol$_U^{-1}$ K^{-2} [19], signaling increased hybridization between 5*f* and conduction electrons across the series [70]. The relative correlation strength is also reflected in the magnitude of the Weiss temperature θ_W, extracted from the magnetic susceptibility data: $\theta_W(U_2Zn_{17}) = -120$ K [71] $< \theta_W(U_{23}Hg_{88}) = -90$ K [see Fig. 3(a) of the present work] $< \theta_W(UCd_{11}) = -42$ K [71]. The estimates of the Kadowaki-Woods $A/\gamma^2 = 0.6\ \mu\Omega$ cm mol$_U^2$ K^2 J^{-2} and Wilson 0.5 <

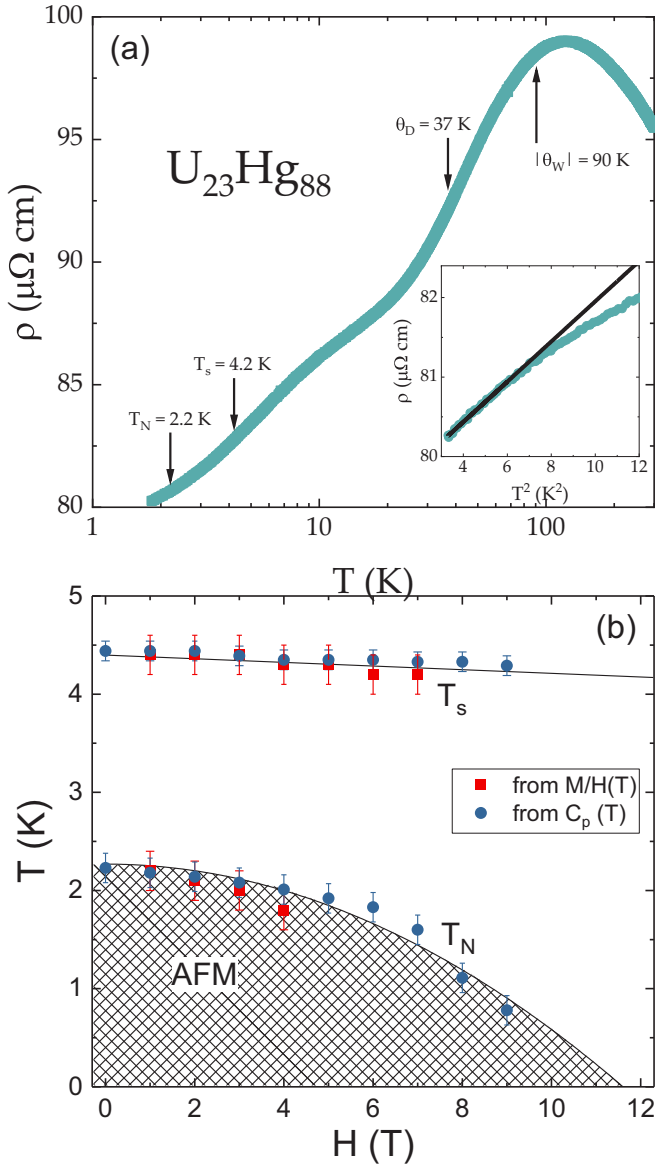

FIG. 5. (a) Resistivity as a function of temperature for $U_{23}Hg_{88}$. The characteristic temperatures are marked by arrows, while the low-temperature T^2 behavior is shown in the inset, along with a linear fit. (b) The *H*-*T* phase diagram of $U_{23}Hg_{88}$: The values of T_N and T_s are extracted from $M(T)$ (squares) and $C_p(T)$ (circles) data.

$\chi_0/\gamma < 1$ (50 K $< T_K <$ 100 K) ratios of $U_{23}Hg_{88}$ are comparable to UCd_{11} and U_2Zn_{17}. This once again highlights the similarity of these peculiar heavy-fermion systems.

While several analogies exist between U_2Zn_{17}, $U_{23}Hg_{88}$, and UCd_{11}, one major difference seems to be the state of the 5*f* electrons. In UCd_{11}, the local moment scenario applies [72], while evidence of itinerant magnetism has been observed in U_2Zn_{17} [63]. $U_{23}Hg_{88}$ displays signatures of both local (large effective magnetic moment) and itinerant (small entropy of the antiferromagnetic transition, reduction of γ below T_N, absence of a corresponding feature in resistivity) magnetism.

In this work, we propose several properties which empirically lead to the significant effective mass enhancement, providing a novel and reliable route in the search for new uranium-based heavy-fermion materials. We postulate that in order to find new uranium-based materials, the following characteristics are beneficial: (i) mass percentage of U should be low, (ii) coordination number of uranium should be high, and (iii) the overall shortest uranium bond should be long. Additionally, complex crystal structures, as evidenced by the large number of atoms per primitive unit cell, should be targeted. This approach was successfully implemented to discover a novel heavy-fermion compound $U_{23}Hg_{88}$. A very large effective mass enhancement is observed in $U_{23}Hg_{88}$, showcasing that its intricate crystallographic properties are closely related to the fascinating physical phenomena it exhibits.

We are grateful to Elena Hassinger, Manuel Brando, Frank Steglich, Zachary Fisk, and Walter Schnelle for fruitful discussions, and to Ralf Koban for his valuable technical support.

[1] G. R. Stewart, Rev. Mod. Phys. **56**, 755 (1984).
[2] G. R. Stewart, Rev. Mod. Phys. **73**, 797 (2001).
[3] G. R. Stewart, Rev. Mod. Phys. **78**, 743 (2006).
[4] H. Löhneysen, A. Rosch, M. Vojta, and P. Wölfle, Rev. Mod. Phys. **79**, 1015 (2007).
[5] S. Wirth and F. Steglich, Nat. Rev. Mater. **1**, 16051 (2016).
[6] M. B. Maple, M. C. de Andrade, J. Herrmann, Y. Dalichaouch, D. A. Gajewski, C. L. Seaman, R. Chau, R. Movshovich, M. C. Aronson, and R. Osborn, J. Low Temp. Phys. **99**, 223 (1995).
[7] H. Löhneysen, Phys. B **206**, 101 (1995).
[8] M. B. Maple, C. L. Seaman, D. A. Gajewski, Y. Dalichaouch, V. B. Barbetta, M. C. de Andrade, H. A. Mook, H. G. Lukefahr, O. O. Bernal, and D. E. MacLaughlin, J. Low Temp. Phys. **95**, 225 (1994).
[9] B. Coqblin, in *Strongly Correlated Electron Behaviors and Heavy Fermions in Anomalous Rare-Earth and Actinide Systems*, AIP Conf. Proc. No. 846 (AIP, New York, 2006).
[10] M. B. Maple, J. Phys. Soc. Jpn. **74**, 222 (2005).
[11] M. B. Maple, R. E. Baumbach, N. P. Butch, J. J. Hamlin, and M. Janoschek, J. Low Temp. Phys. **161**, 4 (2010).
[12] P. A. Lee, N. Nagaosa, and X. G. Wen, Rev. Mod. Phys. **78**, 17 (2006).
[13] E. L. Thomas, J. N. Millican, E. K. Okudzeto, and J. Y. Chan, Comments Inorg. Chem. **27**, 1 (2006).
[14] R. Gumeniuk, A. N. Yaresko, W. Schnelle, M. Nicklas, K. O. Kvashnina, C. Hennig, Y. Grin, and A. Leithe-Jasper, Phys. Rev. B **97**, 174405 (2018).
[15] Z. Fisk, J. L. Sarrao, J. L. Smith, and J. D. Thompson, Proc. Natl. Acad. Sci. USA **92**, 6663 (1995).
[16] G. Zwicknagl and P. Fulde, J. Phys.: Condens. Matter **15**, 1911 (2003).
[17] H. R. Ott, H. Rudigier, P. Delsing, and Z. Fisk, Phys. Rev. Lett. **52**, 1551 (1984).
[18] Y. Hirose, H. Doto, F. Honda, D. Li, D. Aoki, Y. Haga, and R. Settai, J. Phys.: Condens. Matter. **28**, 425601 (2016).
[19] Z. Fisk, G. R. Stewart, J. O. Willis, H. R. Ott, and F. Hulliger, Phys. Rev. B **30**, 6360 (1984).
[20] The vast majority of studies on UBe_{13} have been performed on single crystals, grown out of Al flux. The conflicting values of the critical temperature T_c, the size of the specific heat anomaly, as well as the value of γ, hinted at possible sample quality issues [21–25]. We have recently shown that such drastic variation of the physical properties arises from the incorporation of Al into the lattice, resulting in $UBe_{13-x}Al_x$ [26]. Since the properties of $UBe_{13-x}Al_x$ are similar to $UBe_{13-x}B_x$ [27,28], we use the value of the Sommerfeld coefficient for polycrystalline UBe_{13} samples [29].
[21] R. Corcoran, P. Meeson, P. A. Probst, M. Springford, B. Wolf, R. Blick, G. Bruls, B. Lüthi, Z. Fisk, J. L. Smith, and H. R. Ott, Z. Phys. **91**, 135 (1993).
[22] J. L. Smith, Philos. Mag. **65**, 1367 (1992).
[23] H. R. Ott, E. Felder, A Bernasconi, Z. Fisk, J. L. Smith, L. Taillefer, and G. G. Lonzarich, Jpn. J. Appl. Phys. **26**, 1217 (1987).
[24] N. E. Alekseevskii, A. V. Mitin, E. P. Khlybov, A. Gilevskii, and B. Gren', Zh. Eksp. Teor. Fiz. **45**, 250 (1987).
[25] C. Stassis, J. Arthur, C. F. Majkrzak, J. D. Axe, B. Batlogg, J. Remeika, Z. Fisk, J. L. Smith, and A. S. Edelsteins, Phys. Rev. B **34**, 4382(R) (1986).
[26] A. Amon, I. Zelenina, P. Simon, M. Bobnar, M. Naumann, E. Svanidze, F. Arnold, H. Borrmann, U. Burkhardt, W. Schnelle, E. Hassinger, A. Leither-Jasper, and Yu. Grin, Sci. Rep. **8**, 10654 (2018).
[27] R. H. Heffner, W. P. Beyermann, M. F. Hundley, J. D. Thompson, J. L. Smith, Z. Fisk, K. Bedell, P. Birrer, C. Baines, F. N. Gygax, B. Hitti, E. Lippelt, H. R. Ott, A. Schenck, and D. E. MacLaughlin, Conf. Magn. Magnetic Mater. **36**, 1 (1990).
[28] R. H. Heffner, H. R. Ott, A. Schenck, J. A. Mydosh, and D. E. MacLaughlin, J. App. Phys. **70**, 5782 (1991).
[29] E. Svanidze, M. König, and A. Amon, E. Hassinger, A. Leither-Jasper, A. P. Mackenzie, and Yu. Grin (unpublished).
[30] H. Hill, *Plutonium 1970 and Other Actinides* (AIME, New York, 1970).
[31] B. H. Morrison and R. E. Blanco, USA EC Report **ORNL**, 151, 1956, https://digital.library.unt.edu/ark:/67531/metadc1017949/.
[32] O. C. Dean, E. Sturch, B. H. Morrison, and R. E. Blanco, *Status of the Hermex Process* (Oak Ridge National Laboratory, 1957).

[33] F. L. Culler and H. C. Forsberg, USA EC Report **ORNL**, 62, 1959, https://digital.library.unt.edu/ark:/67531/metadc864823/.

[34] Y. Kobayashi and A. Saito, J. Nucl. Sci. Technol. **12**, 508 (1975).

[35] H. C. Lee, L. C. Wang, H. H. Hung, and C. T. Chang, J. Chem. Soc. Chem. Commun. **124**, 124 (1975).

[36] C. T. Chang, Inorg. Nucl. Chem. **40**, 507 (1978).

[37] T. L. Yu, Y. S. Lee, Y. D. Chuang, and C. T. Chang, J. Nucl. Sci. Technol. **16**, 508 (1979).

[38] Y. Shiokawa, K. Hasegawa, K. Konashi, M. Takahashi, and K. Suzuki, J. Alloys Compd. **255**, 98 (1997).

[39] K. Hasegawa, Y. Shiokawa, M. Akabori, Y. Suzuki, and K. Suzuki, J. Alloys Compd. **271**, 680 (1998).

[40] R. E. Rundle and A. S. Wilson, Acta Crystallogr. **2**, 148 (1949).

[41] B. R. Frost, Vacuum **4**, 368 (1954).

[42] F. A. Rough and A. A. Bauer, Constitution of Uranium and Thorium Alloys, Report No. BMI-1300 (UC-25 Metallurgy and Ceramics, 1958), https://www.osti.gov/servlets/purl/4324513/.

[43] C. Guminski, J. Phase Equilib. **24**, 461 (2003).

[44] D. H. Ahmann, R. R. Baldwin, and A. S. Wilson, The U-Hg System, U.S. Atomic Energy Commission Report CT-2960, USAEC, Washington, DC (Equilibrium Diagram, Experimental, 1945), https://www.osti.gov/biblio/4350148.

[45] A. Misiuk, J. Mulak, A. Czopnik, and W. Trzebiatowski, Bull. Acad. Pol. Sci. **20**, 337 (1972).

[46] P. Chiotti, J. T. Mason, and T. S. Lee, J. Less-Common Met. **66**, 41 (1979).

[47] T. S. Lee, P. Chiotti, and J. T. Mason, J. Less-Common Met. **66**, 34 (1979).

[48] P. Chiotti, Bull. Alloy Phase Diagrams **1**, 106 (1980).

[49] F. Merlo and M. L. Fornasini, J. Less-Common Met. **64**, 221 (1979).

[50] G. Jangg and F. Steppan, Z. Metallk. **56**, 172 (1965).

[51] V. Sechovsky and L. Havela, *Intermetallic Compounds of Actinides* (Elsevier Science Publishers, New York, 1988).

[52] J. S. Kim and G. R. Stewart, Phys. Rev. B **89**, 041103(R) (2014).

[53] Z. Fisk, H. R. Ott, and J. L. Smith, J. Less-Common Met. **133**, 99 (1987).

[54] See Supplemental Material at http://link.aps.org/supplemental/10.1103/PhysRevB.99.220403 for additional information on (i) the sample preparation, characterization, and measurements [73–76] along with the U-Hg binary phase diagram, (ii) crystallographic parameters of $U_{23}Hg_{88}$, as well as (iii) physical properties of UHg_2 and UHg_3.

[55] A. Amon, A. Ormeci, M. Bobnar, L. G. Akselrud, M. Avdeev, R. Gumeniuk, U. Burkhardt, Y. Prots, C. Hennig, A. Leithe-Jasper *et al.*, Acc. Chem. Res. **51**, 214 (2018).

[56] M. L. Fornasini, B. Chabot, and E. Parthe, Acta Crystallogr. **34**, 2093 (1978).

[57] T. Siegrist and Y. L. Page, J. Less-Common Met. **127**, 189 (1987).

[58] J. D. Thompson, A. C. Lawson, M. W. McElfresh, A. P. Sattelberger, and Z. Fisk, J. Magn. Magn. Mater. **76**, 437 (1988).

[59] J. Dshemuchadse and W. Steurer, MRS Proceedings **1517** (2012).

[60] W. Steurer and J. Dshemuchadse, *Intermetallics: Structures, Properties, and Statistics* (Oxford University Press, New York, 2016).

[61] M. E. Fisher, Philos. Mag. **7**, 1731 (1962).

[62] E. Bauer, A. Slebarski, E. J. Freeman, C. Sirvent, and M. B. Maple, J. Phys.: Condens. Matter **13**, 4495 (2001).

[63] C. Broholm, J. K. Kjems, G. Aeppli, Z. Fisk, J. L. Smith, S. M. Shapiro, G. Shirane, and H. R. Ott, Phys. Rev. Lett. **58**, 917 (1987).

[64] G. R. Stewart, Rev. Sci. Instrum **54**, 1 (1982).

[65] D. Aoki, T. Inoue, K. Kindo, N. Suzuki, K. Miyake, Y. Inada, R. Settai, K. Sugiyama, E. Yamamoto, Y. Haga *et al.*, J. Phys. Soc. Jpn. **68**, 3117 (1999).

[66] N. Tateiwa, S. Ikeda, Y. Haga, T. D. Matsuda, E. Yamamoto, K. Sugiyama, M. Hagiwara, K. Kindo, and Y. Onuki, J. Phys. Soc. Jpn. **80**, 014706 (2011).

[67] J. D. Thompson, Z. Fisk, M. W. McElfresh, H. R. Ott, and M. B. Maple, Phys. Rev. B **39**, 2578 (1989).

[68] J. D. Thompson, Phys. B **190**, 61 (1993).

[69] J. D. Thompson, Z. Fisk, and H. R. Ott, J. Magn. Magn. Mater. **54**, 393 (1986).

[70] G. P. Meisner, A. L. Giorgi, A. C. Lawson, G. R. Stewart, J. O. Willis, M. S. Wire, and J. L. Smith, Phys. Rev. Lett. **53**, 1829 (1984).

[71] A. Misiuk, J. Mulak, and A. Czopnik, Bull. Acad. Pol. Sci. **21**, 487 (1973).

[72] F. Nasreen, D. Antonio, D. VanGennep, C. H. Booth, K. Kothapalli, E. D. Bauer, J. L. Sarrao, B. Lavina, V. Iota-Herbei, and S. Sinogeikin, J. Phys.: Condens. Matter **28**, 105601 (2016).

[73] A. Leithe-Jasper, H. Borrmann, and W. Hönle, *MPI CPfS, Scientific Report, Dresden, 2006*, https://www.cpfs.mpg.de/2075708/C_2006-2008.pdf.

[74] *WinXPow (version 2)* (Darmstadt, STOE and Cie GmbH, 2001), https://www.stoe.com/product/software-powder-xrd/.

[75] L. Akselrud and Y. Grin, J. Appl. Crystallogr. **47**, 803 (2014).

[76] M. Nicklas, *Strongly Correlated Systems—Experimental Techniques* (Springer, Berlin, 2015).